The Use of Phase Diagrams and Thermodynamic Databases for Electronic Materials

X.J. Liu, K. Oikawa, I. Ohnuma, R. Kainuma, and K. Ishida

Phase diagrams and a thermodynamic database constructed by the Calculation of Phase Diagrams approach offer powerful tools for alloy design and materials development. This article presents recent progress on the thermodynamic database for micro-solders and copper-based alloys, which is useful for the development of lead-free solders and prediction of interfacial phenomena between solders and the copper substrate in electronic packaging technology. In addition, examples of phase diagram applications are presented to facilitate the development of Co-Cr-based magnetic recording media in hard disks and new ferromagnetic shape-memory alloys.

INTRODUCTION

The Calculation of Phase Diagrams (CALPHAD) method,[1,2] arising from pioneering work in the computer calculation of phase diagrams by Kaufman and Bernstein[3] in 1970, was developed as a result of progress in computer software such as *Thermo-Calc*[4] and *Solgas-mix*.[5] CALPHAD is now widely used in materials design, and thermodynamic databases are available for alloy systems such as Fe, Ni, Ti, Al, Mg-based alloys, ceramic systems, and alloy semiconductors.

Recently, the authors of this article developed thermodynamic databases for micro-soldering materials[6–8] and copper-based alloys[9,10] within the framework of the CALPHAD method. These databases are useful for the design of lead-free solders and copper-based substrate materials as well as for understanding of the interfacial reaction between them. In addition, a thermodynamic database is being constructed for cobalt-based alloys, which is important for such applications as heat- and corrosion-resistant alloys, magnetic alloys, and bio-materials. This article, which focuses on micro-solders, copper-based alloys, Co-Cr magnetic recording media, and Co-Ni-Al ferromagnetic shape-memory alloys, presents the role of phase diagrams and thermodynamic databases in materials design.

A THERMODYNAMIC DATABASE FOR ELECTRONIC MATERIALS

To meet requirements arising from environmental and health issues concerning the toxicity of lead, lead-free solders have been developed during the past decade to replace conventional Pb-Sn alloys.[11] To develop lead-free solders, a thermodynamic database of micro-soldering alloys for reliable

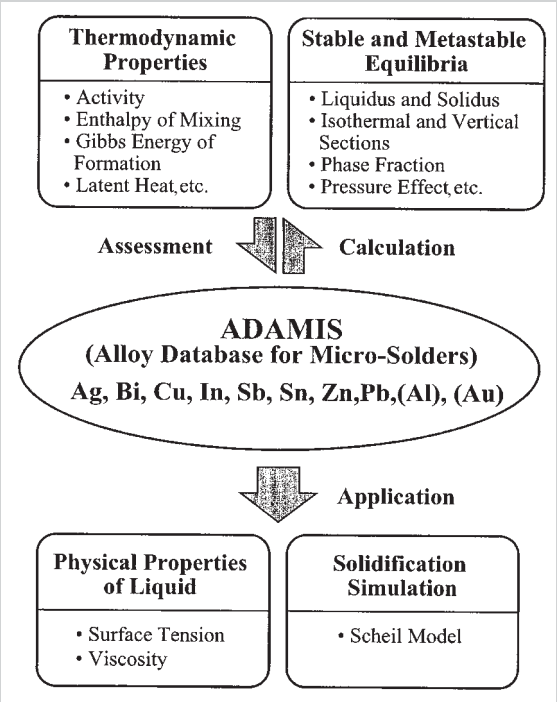

Figure 1. An outline of ADAMIS.

Figure 2. An outline of the application of a thermodynamic database.

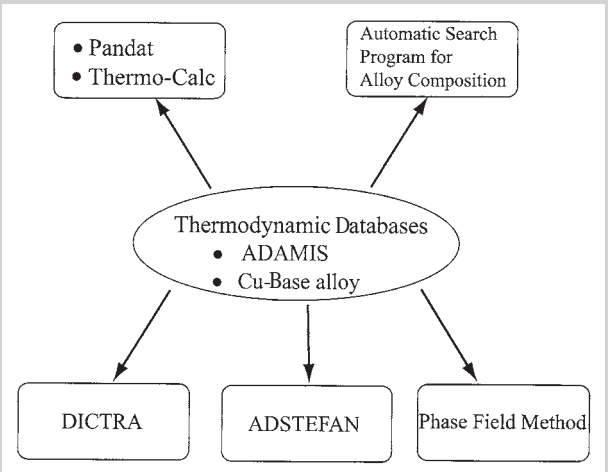

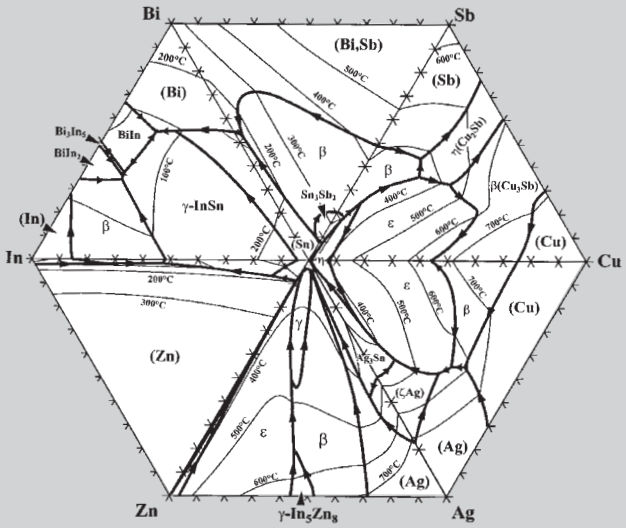

Figure 3. The liquidus surfaces in the tin-based ternary systems.

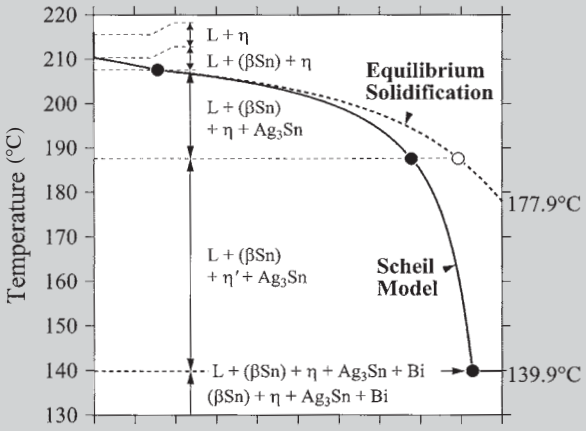

Figure 4. A solidification simulation of the Sn-2.0Ag-0.5Cu-7.5Bi alloy.

predictions of melting and freezing temperatures, as well as of the constituent phases and mole fractions, etc., is required. Such information is difficult to obtain, especially for multicomponent systems. In addition, copper-based substrate materials corresponding to new lead-free solders also need to be developed.

Micro-Soldering Materials and Copper-Based Alloys

A thermodynamic database of micro-soldering materials, Alloy Database for Micro-Solders (ADAMIS), was developed to calculate phase equilibria in the entire composition range for the elements Ag, Bi, In, Cu, Sn, Sb, Zn, and Pb and in a limited composition range for Al and Au.

Alloy Database for Micro-Solders is a thermodynamic tool for design of micro-soldering materials by combining the database with *PANDAT*, a user-friendly multicomponent phase-diagram-calculation software program.[12] Even beginners can easily manage this ADAMIS/*PANDAT* tool through the Windows interface. The calculated results are independent of the user's level of expertise since the program can automatically find starting points and initial values for stable phase equilibria.

Figure 1 shows the main contents of ADAMIS, which provides such information as stable and metastable phase equilibria, projection of the liquidus surface, phase fractions, and simulation of solidification. In addition, ADAMIS can be used to calculate the surface tension and viscosity in the liquid phase. A thermodynamic database of copper-based alloys containing Cu-X binary; Cu-Fe-X, Cu-Cr-X, and Cu-Ni-X ternary; and Cu-Ni-Cr-Sn-Zn-Fe-Si multicomponent systems has also been developed.[9,10] To obtain a reliable assessment of thermodynamic parameters, experimental investigations of phase equilibria including not only first-order phase transformation but also order-disorder transition for some important systems with no or very little experimental data were carried out.

APPLICATION OF THERMODYNAMIC DATABASE

The thermodynamic database of micro-soldering materials and copper-based alloys can be combined with other software programs and various simulations can be conducted. Figure 2 shows an outline of the application of databases that not only provide thermodynamic information on phase equilibria by using the *Thermo-Calc* and *PANDAT* software programs, but also yield information on the kinetics and microstructure evolution.

Design of Micro-Soldering Materials

Melting temperature is one of the most basic factors in the development of suitable alternatives to Pb-Sn solders. Significant efforts have been made to design tin-based solders, and Figure 3 shows the liquidus projection of some tin-based ternary systems in which the isothermal lines and reaction types are indicated. The solidification process of solders is also an important factor in the design of lead-free solders. Although the Scheil model assumes that local equilibrium exists at the liquid/solid

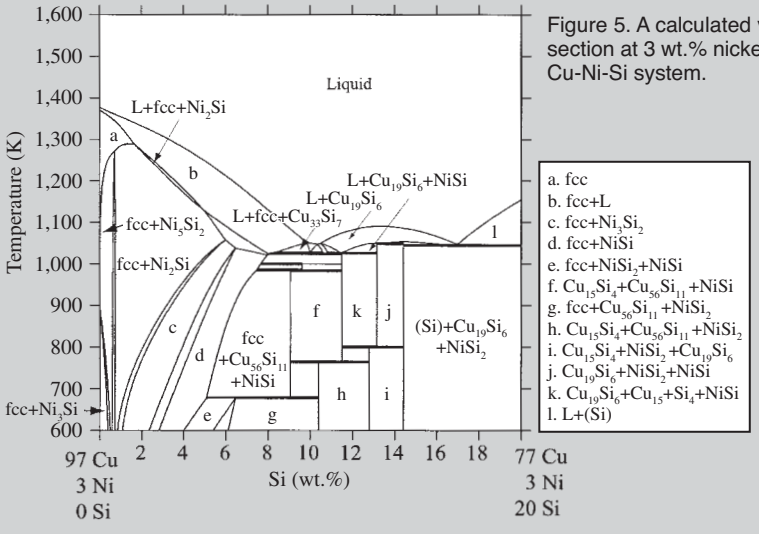

Figure 5. A calculated vertical section at 3 wt.% nickel in the Cu-Ni-Si system.

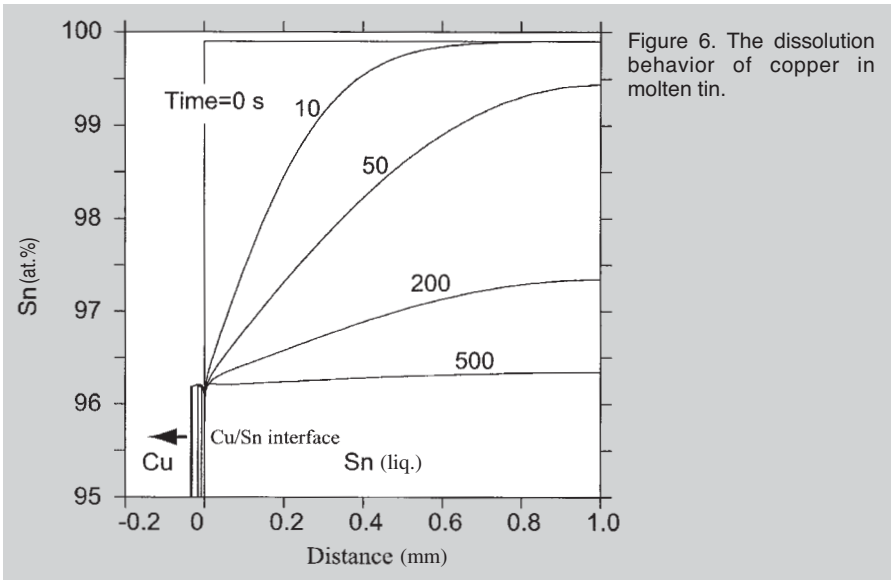

Figure 6. The dissolution behavior of copper in molten tin.

interface and that diffusion is absent in the solid phase, such calculation can still provide a prediction close to reality. A solidification simulation was carried out for a promising candidate as an alternative to Pb-Sn solders, the Sn-2.0Ag-0.5Cu-7.5Bi (wt.%) alloy. Figure 4 shows the variation of the calculated mass fraction of the solid phase with temperature in this alloy under equilibrium and Scheil model solidification conditions. In both cases, solidification starts with the primary crystals of η-Cu_6Sn_5 and the liquid phase disappears at 177.9°C under the equilibrium solidification conditions. However, according to the Scheil model, bismuth is concentrated in the liquid phase during solidification, which causes an extensive fall of the terminating temperature of solidification (139.9°C) corresponding to the eutectic reaction of the Sn-Bi binary system.

The surface tension and viscosity of the liquid phase, which are relevant to the soldering process, can be predicted from the Gibbs energy of liquid by combining the appropriate models.[13,14]

Copper-Based Alloys

High-strength copper-based alloys with high electrical conductivity have been used for such electronic devices as substrates, connectors, and springs. These copper alloys are developed by utilizing precipitation hardening of the face-centered cubic (fcc) phase. A typical example of phase equilibria of age-hardened copper-based alloys is presented in Figure 5, which shows the calculated vertical section diagram at 3 wt.% nickel in the well-known Corson alloy system Cu-Ni-Si. It is seen that Ni_5Si_2, Ni_2Si, and Ni_3Si compounds may precipitate from the fcc phase during cooling due to the addition of a small amount of silicon.

Simulation of Copper Dissolution in Molten Solders

The dissolution reaction between a substrate and solders is important for the reliability of electronic packaging. Such a problem can be predicted by combining the thermodynamic database with *Diffusion Controlled Transformation* (*DICTRA)* software,[15] in which the kinetic parameters are assessed on the basis of various diffusion coefficients in the liquid and fcc phases.[16] As an example, for a diffusion couple of copper (solid)/tin (liquid) heat treated at 250°C for different lengths of time, a simulation of the dissolution behavior of copper in molten tin was carried out.[9,16] In Figure 6, which shows the change of the concentration of copper in liquid tin with increasing time, the concentration of the liquid phase almost reaches the equilibrium composition in about 500 s. In addition, movement of the Cu/Sn (liquid) interface to the copper side can be observed.

Simulation of Solidification Process

The evolution of microstructure during solidification, which is essential for understanding lift-off phenomena,[17,18] can be quantitatively predicted by the phase-field method.[19,20] Ode et al. have applied phase-field simulation to microstructure evolution during solidification of the Sn-5Bi alloy in reflow soldering.[9,21]

The simulation results of microstructure evolution during solidification at the tilted angles of 45° and 0° are shown in Figure 7, respectively, corresponding to the microstructures at 3 s after solidification. Figure 7a shows that the tip of the dendrite for the tilted angle of 45° is slightly bent at the land due to the solute enrichment. When the tilted angle is 0°, however, the tip of the primary dendrite approaches the land without bending (Figure 7b), and the secondary dendrite arms grow along the land surface. The results show that micro-segregation does not always prevent the growth of the solid in the vicinity of the land.

Lead-Free Solder Ball with Core Structure

Compared with more conventional packages, the ball grid array (BGA) package has the advantages of higher input/output terminal density, a smaller footprint, and higher reliability.[22] In particular, copper core solders plated with a Pb-Sn eutectic alloy for BGA joints have been developed and used.[23] In recent studies, an egg-type powder with a core microstructure was obtained from alloy systems possessing a liquid miscibility gap.[24] The authors of this

a b

Figure 7. The microstructural evolution in the fillet above the copper surface. (a) Tilted angle: 45°, time: 0.3 s and (b) tilted angle: 0°, time: 0.38 s.

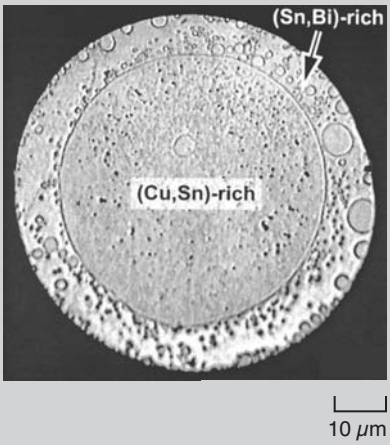

Figure 8. The egg-type microstructure of Cu-15Sn-50Bi (wt.%) alloy powder.

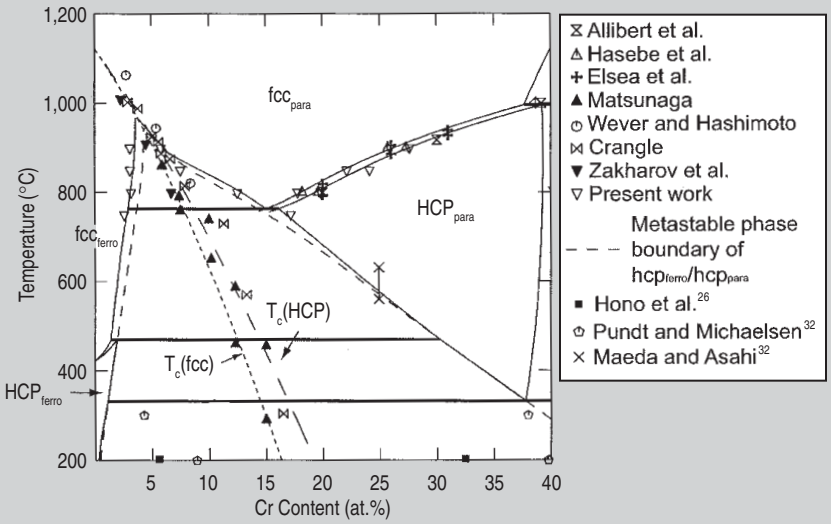

Figure 9. A phase diagram of cobalt-rich portion in the Co-Cr binary system.

article developed a promising BGA ball consisting of a copper-based core with a lead-free low-melting solder periphery designed by ADAMIS. A powder of Cu-15Sn-50Bi was prepared using conventional nitrogen gas atomization under an argon atmosphere, where a stable liquid miscibility gap appeared as predicted by ADAMIS. Figure 8 shows the microstructure of this alloy powder, clearly indicating the egg-type structure of the Cu-Sn-rich core with a Bi-Sn-rich periphery. The commercial size of the copper-core ball plated with Pb-Sn eutectic solder is about 700 μm, but a size less than 100 μm, which is very difficult to produce by the conventional plating method, is required for the chip-scale package. As shown in Figure 8, the size of the egg-type powder is about 80 μm, which should be an attractive ball for electronics packaging technology in the future.

DESIGN OF NEW FUNCTIONAL MATERIALS

Co-Cr-Based Magnetic Recording Media

Co-Cr-based sputtered thin films have a high coercivity (Hc) with a high magnetization (M) and have been widely used as magnetic recording media of hard disks.[25] The thin films have a hexagonal close-packed (hcp) structure and a fine microstructure with the cobalt-rich ferromagnetic phase precipitated in the chromium-rich paramagnetic matrix.[26] The distribution of chromium in each phase and the microstructure have a significant effect on the recording properties of this alloy. Ishida and Nishizawa[27] have suggested that a likely origin of the chromium segregation in a Co-Cr alloy thin film is the miscibility gap in the hcp phase because the thermodynamic calculations of the Co-Cr binary system by Hasebe et al.[28] indicates a magnetically induced miscibility gap in fcc and hcp phases along the Curie temperature. This suggestion is now generally accepted by other researchers. However, the experimental confirmation of the miscibility gap in a bulk sample has not yet been obtained because of experimental difficulties. Recently, Oikawa et al. confirmed the miscibility gap along the Curie temperature in several cobalt-based fcc alloys by the diffusion-couple technique and reevaluated the thermodynamic properties.[29–31] The phase diagram in the cobalt-rich corner of the Co-Cr system is shown in Figure 9 together with the experimental results for thin films.[26,32,33] The calculated metastable magnetically induced phase separation in the hcp phase agrees well with the experimental results, strongly

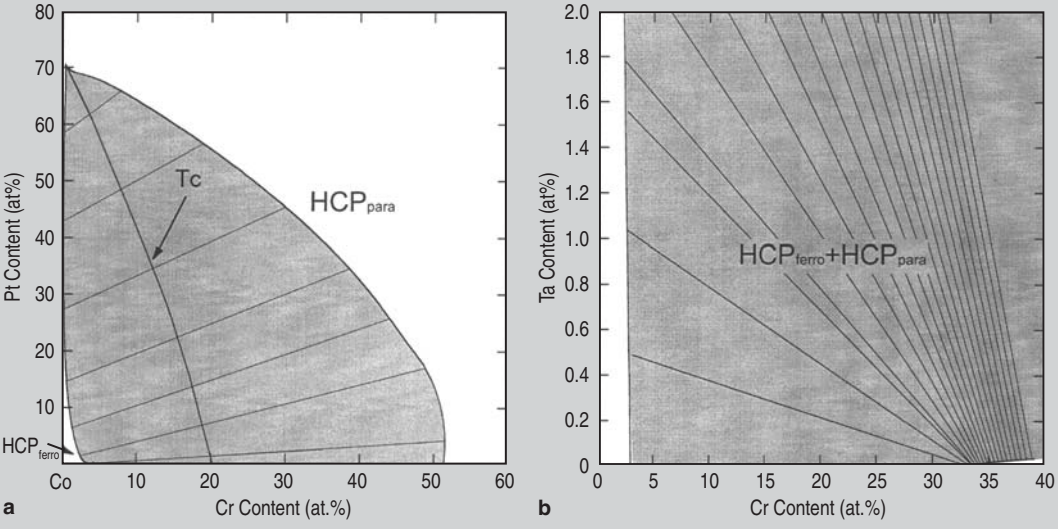

Figure 10. The phase equilibria of (a) a Co-Cr-Pt system at 200°C and (b) a Co-Cr-Ta system at 400°C.

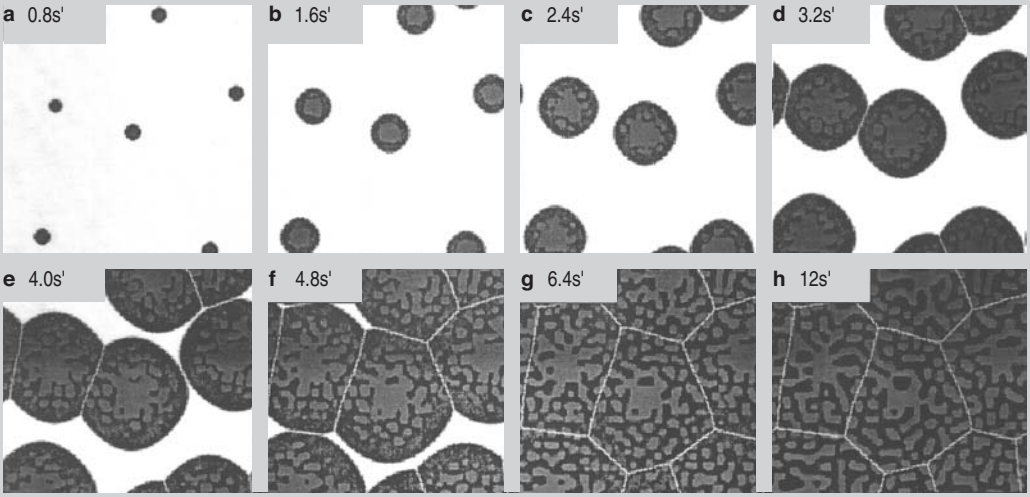

Figure 11. The microstructural evolution of Co-22 at.%Cr film at 200°C by phase-field method.

implying that the magnetically induced phase separation is responsible for the compositional heterogeneity in Co-Cr-based films.

It is well known that the addition of platinum and/or tantalum to Co-Cr-based high-density magnetic recording media modifies the recording characteristics, resulting in a drastic change in the distribution of chromium.[34,35] The thermodynamic calculation of the magnetically induced phase separation in the hcp phase of Co-Cr-Pt and Co-Cr-Ta ternary systems has been conducted to explain the effect of the addition of platinum and tantalum on the chromium distribution in the Co-Cr-based alloys.[36,37] The calculated miscibility gap in the hcp phase including the metastable phase boundaries is shown in Figure 10, with the isothermal section of the Co-Cr-Pt system at 200°C shown in Figure 10a.[36] The miscibility gap is formed along the Curie temperature, and the width of the gap of the Co-Cr binary becomes narrower with increasing platinum content. Kitakami et al.[38] have investigated the effect of platinum on the magnetic properties of Co-Cr thin films and concluded that the addition of platinum enhances the magnetic anisotropy energy (MAE) with a large coercivity because such addition reduces the chromium content in the cobalt-rich ferromagnetic phase. The calculated results reveal that the chromium content in the ferromagnetic hcp phase decreases with increasing platinum content, as shown in Figure 10a, which agrees well with the experimental data.[26,34] The isothermal section of the Co-Cr-Ta system at 400°C is shown in Figure 10b.[37] The two-phase region is extended with increasing tantalum content and the chromium segregation is enhanced, whereas the chromium content in the ferromagnetic phase is not drastically reduced. This tendency qualitatively agrees with the results of the experimental data of Co-Cr-based thin films.[34,39] The thermodynamic assessment of Co-Cr systems allows simulation of the microstructural evolution by combining it with the phase-field method. Figure 11 shows how the modulated structure is formed in the Co-22at.%Cr alloy at 200°C.[40]

From the thermodynamic calculation of the Co-Cr-X ternary system, the shape of the magnetically induced phase separation in the cobalt-rich portion can be classified into four types, as shown in Figure 12.[41] In Type I, the chromium contents in both the ferromagnetic and paramagnetic phases decrease with an increasing amount of X. In Type II, the chromium content decreases in the ferromagnetic phase and increases in the paramagnetic phase with an increasing amount of X. In Type III, the chromium content of the paramagnetic phase is increased by the addition of X, whereas that in the ferromagnetic phase is not effectively reduced. Finally, in Type IV, the three-phase equilibrium of one ferromagnetic and two paramagnetic phases is formed. Figure 13 shows the classification of the effect of the alloying elements on the phase equilibria of the Co-Cr system in the periodic table based on the calculated results. Pd, Rh, and Ir show a type of miscibility gap similar to that of the Co-Cr-Pt phase diagram. The magnetic properties of the Co-Cr-Pd thin-film alloy would be expected to be similar to those of the

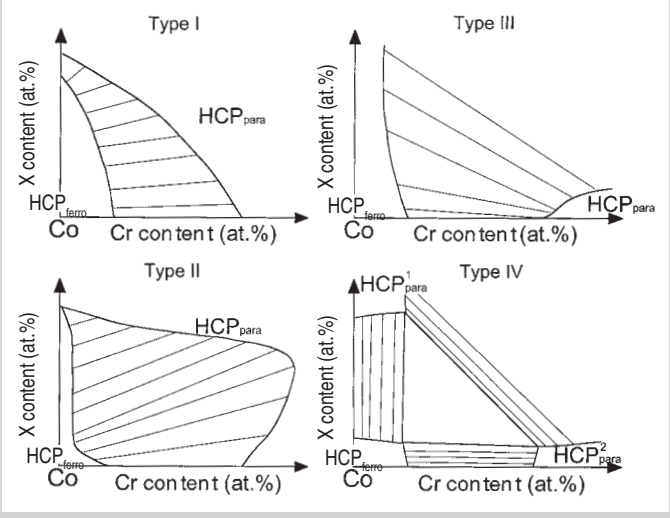

Figure 12. The classification of phase separation in the hcp phase of the Co-Cr-X ternary system.

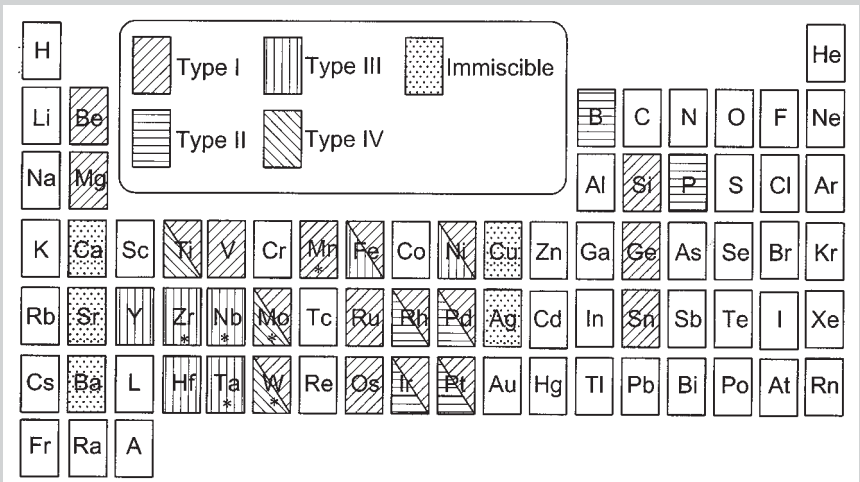

Figure 13. The effect of alloying elements on the phase separation of the Co-Cr binary system.

Co-Cr-Pt system. On the other hand, the addition of iridium to cobalt strongly decreases the MAE, which in turn would cancel out the beneficial effect of decreasing chromium content in the ferromagnetic phase by the alloying of iridium.[42] This means that the MAE of each binary system, as well as the phase diagram, should be considered for the material design of Co-Cr-based high-density magnetic recording media.

Recently, the authors proposed thin films with a Co-Mo-based hcp structure as promising candidates for high-density recording media. In these thin films, the magnetically induced phase separation of the hcp phase was predicted by thermodynamic calculation and a large MAE was measured.[43] The development of the compositional fluctuation of molybdenum in Co-Mo sputtered thin films prepared on a heated substrate was confirmed by an analytical transmission-electron microscope equipped with an energy-dispersive x-ray analyzer. The fluctuation may have been caused by magnetically induced phase separation in analogy with Co-Cr-based thin films.

New Ferromagnetic Shape Memory Alloys

Ferromagnetic shape-memory alloys (FSMAs) have received much attention as high-performance magnetically controlled actuator materials because they show a large magnetically induced strain by the rearrangement of twin variants in the martensite.[44] Several candidates for FSMAs have been reported, including Ni_2MnGa,[44] Fe-Pd,[45] and Fe_3Pt[46] alloys. Recently, the authors found a new group of FSMAs in Co-Ni-Al β (B2 structure)-based alloys.[47–49]

The Curie temperature (Tc), the martensitic transformation starting temperature (Ms), and the reverse-transformation finishing temperature (Af) are plotted as a function of the cobalt content in the 30 at.% aluminum section, as shown in Figure 14.[49] The alloys show thermoelastic martensitic transformation from the β to β′ ($L1_0$ structure) accompanied by the shape-memory effect. Ms increases and Tc decreases with increasing nickel content. The phase-transformation behavior of the alloys on cooling can be grouped into three types based on the characteristic features of the magnetic and martensitic transformations. In Type I, the paramagnetic β phase is magnetically transformed into the ferromagnetic β phase, and then martensitically transformed into the ferromagnetic β′ phase (i.e., T_C^{β}>Ms). In Type II, the paramagnetic β′ phase is directly transformed into the ferromagnetic martensite β′ phase (i.e., T_C^{β}<Ms<$T_C^{\beta'}$). In Type III, the paramagnetic β phase is martensitically transformed into the paramagnetic β′ phase and eventually ferromagnetic transition occurs in the β′ phase (i.e., $T_C^{\beta'}$<Ms). In the case of Type I alloys, the magnetization drastically increases and decreases at As and Ms temperatures,[47] respectively. A large MAE of Ku = $3.9*10^6$ erg/cm^3 was confirmed in the martensite phase of the Co-Ni-Al β single crystal,[48] being the same order of that of Ni_2MnGa. In the case of Type II alloys, the magnetization drastically decreases and increases at As and Ms temperatures,[49] respectively. This is due to the difference in the Curie temperature between the β and β′ phases.

The presence of the fcc-γ solid solution as a second phase in the NiAl-β-based alloy system rendered the alloy ductile[50] and developed β + γ two-phase shape-memory alloys in the NiAl-β-based system including Fe, Co, and Mn.[51–53] The contours of iso-Ms and iso-Tc lines drawn on the basis of the experimental data are shown in Figure 15 together with the phase boundaries of β + γ at 1,100°C and 1,300°C of the Co-Ni-Al ternary system.[47,53,54] The composition range of the β–phase alloy exhibiting the FSME is located near the β + γ two-phase boundary. The β + γ two-phase FSMAs can be produced by a suitable choice of alloy composition and annealing temperature. The $Co_{40}Ni_{33}Al_{27}$ alloy was investigated as a typical β + γ two-phase FSMA.[47] The ductility of the alloy can be significantly improved by the introduction of about 7 vol.% γ phase, as reported in other NiAl-β-based alloys, although the β single-phase polycrystalline alloys as well as the Ni_2MnGa show poor ductility. The shape-memory effect in the ferromagnetic state of the β + γ two-phase FSMA was examined by a simple bending test. A 150 μm thick specimen of the two-phase alloy was annealed at 1,350°C for 2 min. and at 1,300°C for 15 min. The thin plates were bent to realize a surface strain of 2% at Ms (–13°C). Upon heating above Af to 26°C, shape

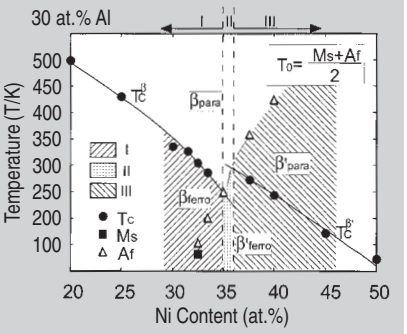

Figure 14. The compositional dependence of the Curie temperature (Tc), the martensitic transformation temperature (Ms), and the austenite finishing temperature (Af) in $Ni_{70-X}Co_XAl_{30}$ alloys.

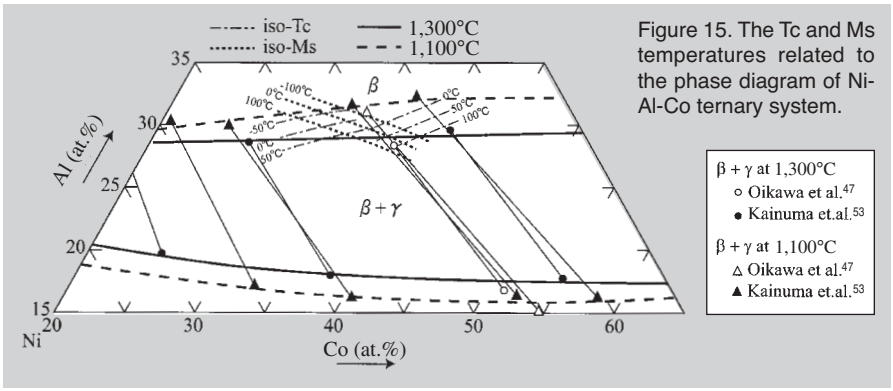

Figure 15. The Tc and Ms temperatures related to the phase diagram of Ni-Al-Co ternary system.

recovery of about 83% was obtained.

Recently, the authors proposed other new FSMAs in Co-Ni-Ga,[49] Ni-Al-Fe,[55] and Ni-Ga-Fe[56,57] systems belonging to the same group as the β-based FSMAs in the Co-Ni-Al system. The ductility of these new FSMAs can also also improved by the introduction of a small amount of γ phase in analogy with the Co-Ni-Al two-phase FSMAs.

ACKNOWLEDGEMENTS

This work was supported by a grant-in-aid for scientific research from the Ministry of Education, Science, Sports, and Culture, Japan, and a grant-in-aid for the Development of Innovative Technology and Nanotechnology Project, Japan.

References

1. T. Nishizawa, *Mater. Trans. JIM,* 33 (1992), p. 713.
2. N. Saunders and A.P. Miodownik, *CALPHAD* (Lausanne, Switzerland: Pergamon, 1998).
3. L. Kaufman and H. Bernstein, *Computer Calculation of Phase Diagrams* (New York: Academic Press, 1970).
4. B. Sundman, B. Jansson, and T.O. Anderson, *CALPHAD,* 9 (1985), p. 153.
5. G. Eriksson and K. Hack, *CALPHAD,* 8 (1984), p. 15.
6. I. Ohnuma et al., *J. Electron. Mater.,* 28 (1999), p. 1163.
7. I. Ohnuma et al., *Functional Materials,* ed. K. Grassie et al. (Weinheim, Germany: Wiley-VCH, 2000), p. 69.
8. X.J. Liu et al., *Mechanics and Materials Engineering for Science and Experiments,* ed. Y.C. Zhou, Y.X. Gu, and Z. Li (New York: Science Press, 2001), p. 334.
9. X.J. Liu et al., *J. Electron Mater,* 32 (11) (2003), pp. 1265–1272.
10. C.P. Wang et al., to be submitted to *J. Phys. Chem. Solids*.
11. P.T. Vianco and D.R. Frear, *JOM,* 45 (7) (1993), pp. 14–18.
12. S.L. Chen et al., *J. Phase Equilibria,* 22 (2001), p. 373.
13. J.A.V. Butler, *Proc. Roy. Soc.,* A135 (1932), p. 348.
14. S. Seetharaman and S. Sichen, *Metall. Mater. Trans. B,* 25B (1993), p. 89.
15. J.O. Andesson et al., *Fundamental and Application of Ternary Diffusion,* ed. G.R. Purdy (New York: Pergamon Press, 1990), p. 153.
16. X.J. Liu et al., *J. Iron Steel International,* 6 (2002), p. 333.
17. H. Takao and H. Hasegawa, *J. Electron. Mater.,* 30 (2001), p. 1060.
18. K. Suganuma et al., *Acta Mater.,* 40 (2000), p. 4475.
19. W.J. Boettinger et al., *Ann. Rev. Mater. Res.,* 32 (2002), p. 163.
20. M. Ode, S.G. Kim, and T. Suzuki, *ISIJ International,* 41 (2001), p. 1076.
21. M. Ode et al., 32 (12) *J. Electron. Mater.* (2003).
22. E. Bradley and K. Banerji, *IEEE Trans. Comp. Pkg. & Mfg. Technol.,* B19 (1996), p. 320.
23. S. Kiyono et al., *J. Jpn. Electron. Packaging,* 2 (1999), p. 298.
24. C.P. Wang et al., *Science,* 297 (2002), p. 990.
25. D. Weller and M. FeDoerner, *Ann. Rev. Mater. Sci.,* 30 (2000), p. 661.
26. K. Hono et al., *Appl. Phys. Lett.,* 62 (1993), p. 2504.
27. K. Ishida and T. Nishizawa, *Proc. Inter. Conf. on User Aspects of Phase Diagrams,* ed. F.H. Hayes (London: The Inst. Metals, 1991), p. 185.
28. M. Hasebe, K. Oikawa, and T. Nishizawa, *J. Jpn. Inst. Metals* (in Japanese), 46 (1982), p. 577.
29. K. Oikawa et al., *Acta Mater.,* 50 (2002), p. 2223.
30. G.W. Qin et al., *J. Magn. Magn. Mater.,* 241 (2002), p. L1.
31. K. Oikawa et al., *J. Magn. Magn. Mater.,* 239 (2002), p. 409.
32. A. Pundt and C. Michaelsen, *Phys. Rev. B,* 56 (1997), p. 14352.
33. Y. Maeda and M. Asahi, *IEEE Trans. Magn.,* MAG-23 (1987), p. 2061.
34. N. Inaba et al., *J. Magn. Magn. Mater.,* 168 (1997), p. 222.
35. Y. Hirayama et al., *IEEE Trans. Magn.,* MAG-32 (1996), p. 3807.
36. K. Oikawa et al., *J. Magn. Magn. Mater.,* 236 (2001), p. 220.
37. K. Oikawa et al., *J. Magn. Soc. Jpn.,* 25 (2001), p. 478.
38. O. KItakami et al., *J. Magn. Magn. Mater.,* 202 (1999), p. 305.
39. R.D. Fisher, J.C. Allan, and J.L. Pressesky, *IEEE Trans. Magn.,* 22 (1986), p. 352.
40. T. Koyama and H. Onodera, private communication (2003).
41. K. Oikawa et al., *Appl. Phys. Lett.,* 79 (2001), p. 644.
42. N. Kikuchi et al., *J. Phys. Condens. Mater.,* 11 (1999), p. L485.
43. K. Oikawa et al., *Appl. Phys. Lett.,* 83 (2003) p. 966.
44. K. Ullakko et al., *Appl. Phys. Lett.,* 69 (1996), p. 1966.
45. R.D. James and M. Wuttig, *Philos. Mag.,* A77 (1998), p. 1273.
46. T. Kateshita et al., *Mater. Trans. JIM,* 41 (2000), p. 882.
47. K. Oikawa et al., *Appl. Phys. Lett.,* 79 (2001), p. 3290.
48. H. Morito et al., *Appl. Phys. Lett.,* 81 (2002), p. 1657.
49. K. Oikawa et al., *Mater. Trans.,* 42 (2001), p. 2472.
50. K. Ishida et al., *Metall. Trans.,* 22A (1991), p. 441.
51. R. Kainuma, K. Ishida, and T. Nishizawa, *Metall. Trans.,* 23A (1992), p. 1147.
52. R. Kainuma et al., *Mater. Res. Soc. Proc.,* 246 (1992), p. 403.
53. R. Kainuma et al., *Intermetallics,* 4 (1996), p. S151.
54. K. Oikawa et al., *J. Phys. IV,* 81 (2003), in press.
55. K. Oikawa et al., *Trans. Mater. Res. Soc. Jpn.,* 28 (2003), p. 263.
56. K. Oikawa et al., *Mater. Trans.,* 43 (2002), p. 2360.
57. K. Oikawa et al., *Appl. Phys. Lett.,* 81 (2002), p. 5201.

X.J. Liu and R. Kainuma are associate professors, I. Ohnuma is a research associate, and K. Ishida is a professor with the Department of Materials Science at Tohoku University. K. Oikawa is a senior researcher at the National Institute of Advanced Industrial Science and Technology in Sendai, Japan.

For more information, contact K. Ishida, Tohoku University, Department of Materials Science, Graduate School of Engineering, Aoba-yama 02, Sendai 980-8579, Japan.